

Multifractal Collision Spectrum of Ballistic Particles with Fractal Surfaces

S. B. Santra^{1,2} and B. Sapoval¹

¹ *Laboratoire de Physique de la Matière Condensée,
Ecole Polytechnique, 91128 Palaiseau Cédex, France.*

² *Department of Physics, Indian Institute of Technology Guwahati, Guwahati-781039, Assam, India.*

(Dated: November 21, 2018)

Ballistic particles interacting with irregular surfaces are representative of many physical problems in the Knudsen diffusion regime. In this paper, the collisions of ballistic particles interacting with an irregular surface modeled by a quadratic Koch curve, are studied numerically. The q moments of the source spatial distribution of collision numbers $\mu(x)$ are characterized by a sequence of “collision exponent” $\tau(q)$. The measure $\mu(x)$ is found to be multifractal even when a random micro-roughness (or random re-emission) of the surface exists. The dimensions $f(\alpha)$, obtained by a Legendre transformation from $\tau(q)$, consist of two parabolas corresponding to a trinomial multifractal. This is demonstrated for a particular case by obtaining an exact $f(\alpha)$ for a multiplicative trinomial mass distribution. The trinomial nature of the multifractality is related to the type of surface macro-irregularity considered here and is independent of the micro-roughness of the surface which however influence the values of α_{min} and α_{max} . The information dimension D_I increases significantly with the micro-roughness of the surface. Interestingly, in contrast with this point of view, the surface seems to work uniformly. This correspond to an absence of screening effects in Knudsen diffusion.

I. INTRODUCTION

Multifractals appear in a wide range of situations like energy dissipation in turbulent flows [1], electronic eigenstates at metal insulator transition [2], fluctuations in finance [3], dynamics of human heartbeat [4] and many others. Recently, multifractal behavior of the first passage time has been studied in the transport of diffusing particles on a 2D Sierpinski gasket with absorbing and reflecting barriers [5]. Our interest is to investigate the multifractal properties associated with the collision spectrum of ballistic trajectories of point particles interacting with irregular surfaces.

The emergence of the concept of fractal geometry has provided an efficient tool to model the influence of strong geometrical irregularity on various physical and chemical processes [6]. Ballistic trajectories in systems with irregular geometry are representative of several physical situations. For example, they correspond to the path of light rays in irregular structures when diffraction phenomena can be neglected. They also represent the path of atoms or molecules in confined vessels at sufficiently low pressure, *i.e.*; in the Knudsen diffusion regime [7]. The interaction of atoms or molecules with irregular surfaces plays a major role in heterogeneous catalysis [8] where porous catalysts have often very irregular surfaces down to the molecular scale. Due to the geometrical irregularity, the small scale structure may confine reactants and increase the interaction with the surface. Xenon nuclear magnetic resonance is used to probe porous structures through the interaction of rare gas atoms with the solid surfaces [9]. The properties of ballistic trajectories in 2D pre-fractal surfaces has already been studied in connection with the chaotic aspects, possibility of “open” black body, Knudsen diffusivity, mean interaction, and catalytic efficiency by Santra et al[10]. Coppens and co-workers have also investigated the influence of the 3D fractal surface morphology on Knudsen diffusion in nanoporous media [11]. Multifractality has already been observed in the molecular diffusion on random fractal structures with time-dependent random potential [12].

The interest here is to explore the multifractal aspects of the number of collisions made by 2D ballistic trajectories within irregular surfaces in the Knudsen diffusion regime. The spatial distribution of the collision numbers of these ballistic trajectories over the slit source is found to be multifractal.

II. THE MODEL

The macro-irregularity of the surface is modeled by a quadratic Koch curve of fractal dimension $\ln 5/\ln 3$. The pre-fractal generator is shown in Fig.1 (a). Particles are launched from a slit of unit length, placed at an angle ϕ with the zeroth order of the pre-fractal. The particle trajectories due to specular collisions within the third ($\nu = 3$) generation of the pre-fractal are shown in Fig.1 (b). Solid lines with an arrow at the end represent the trajectories. The slit source is represented by a thick line extended from $x = 0$ to $x = 1$ placed at $\phi = 45^\circ$ with the zeroth stage of the pre-fractal surface, a horizontal line.

A multifractal measure is in general related to the distribution of a physical quantity on a geometrical support [13]. Here, the geometrical support is the slit source from which the trajectories are launched and the multifractal measure $\mu(x)$ is the distribution of the relative collision numbers, ratio of the number of collisions made by a particle to the total number of collisions made by all the particles, over the slit. The particles leave the slit normally. Each trajectory is followed as long as they are within the pre-fractal surface. A particle trajectory is described by the successive collisions with the surface. The collision points are determined by solving the linear equations describing the particle trajectory and the elements of the pre-fractal surface. The trajectories in Fig.1(b) are generated using this algorithm.

For the pre-fractal ν th generation, the slit is divided into 3^ν equal segments of length $1/3^\nu$ each. A particle is placed at the center of each small part. There are then 3^ν particles launched from the slit. The number of collisions $n(x)$ made by a particle initiated from the position x is counted and the relative collision number $\mu(x)$, ratio of $n(x)$ to the total number of collisions $\sum_x n(x)$ made by all the particles, is then calculated. The value $\mu(x)$ is assigned to the slit segment positioned at x .

Generally, particle reflections with surfaces at finite temperatures are non specular and the angle of reflection, or re-emission θ_r is different from the angle of incidence θ_i . Due to the interaction with the surface, the angle of reflection has a distribution around the angle of incidence. Also the reflection angle could be arbitrary due to the micro-roughness of the surface. Non-specular reflection for atoms or molecules may come from the complex nature of the particle-wall interaction [14]. At the time of hitting the surface, the particle may stay adsorbed for some time and then may desorb, exchanging momentum with the surface. For this reason, the particle trajectories as a whole have a random character. In order to mimic the random character of each collision, the angle of reflection θ_r is supposed to be related to the angle of incidence θ_i as

$$\theta_r = \theta_i + \delta\theta \quad (1)$$

where $\delta\theta$ is a random angle distributed uniformly over a range of angle $\pm\Gamma^\circ$. This range describes qualitatively the random character of the collisions and Γ can also be called the surface micro-roughness. In the following, the Γ values are expressed in units of degree. A few non-specular trajectories computed using the above rule, are shown in Fig.1(c).

In the case of specular reflections, the reflection angle is not determined from numerical computation of trigonometric functions since the elements of the pre-fractal geometry are just parallel to the x and y axes. Consequently, there is no numerical error due to truncation of angle computations. The only truncation errors come from the solution of the linear equations. Because of this error, there could exist trajectories, besides real ray splitting between close trajectories hitting salient corners, which are modified by a ‘‘spurious’’ splitting due to number truncation. To avoid spurious beam splitting, the cumulative error on the point of collision due to the numerical precision of the computer is calculated. For specular reflections, the initial positions of the particles are chosen in such a way that this error is always less than the distance between the point of collision and the nearest corner. For non-specular reflections, those trajectories are rejected and the particles are resent from the same position with a new random number sequence.

It should be emphasized that for $\phi = 45^\circ$, the number of specular reflections for the particular Koch curve considered here can be determined from a simple recursion relation without solving the linear equations for the trajectory and the surface elements. The number of collisions up to the third generations of the pre-fractal surface are listed in Table 1. In the first generation, all the particles send from the central part of the slit have 3 collisions whereas the particles from the other two parts have only 1 collision each. The collision numbers are then in the form of (1,3,1) in the first generation. In the next pre-fractal generation, each part of the the slit is again subdivided into another 3 parts. It can be seen that for $\nu = 2$, the collision numbers (3,9,3) for the particles launched from the central part of the slit is just $3 \times (1,3,1)$ where 3 is the number of collisions corresponding to the same part of the slit for the previous generation. The other two sequences (1,3,1) for the two other parts of the slit are given by $1 \times (1,3,1)$. The trajectories from these two parts had a single collision each at the previous generation. The multiplication of the collision numbers from the first to the second generation of the pre-fractal is shown in Fig.2. Thus, the number of collisions at any two consecutive pre-fractal generations are given as:

$$\begin{array}{l} \nu : \quad \quad \quad n_1, \quad \quad n_2, \quad \quad n_3, \quad \quad \dots, \quad \quad n_n \\ \nu + 1 : \quad \quad n_1, 3n_1, n_1, n_2, 3n_2, n_2, n_3, 3n_3, n_3, \dots, n_n, 3n_n, n_n \end{array} \quad (2)$$

A recursion relation for the collision numbers for $\nu + 1$ generation then can be written as

$$(n_1, n_2, n_3)_{\nu+1} = n_\nu \times (1, 3, 1) \quad (3)$$

where n_ν is the number of collisions of the trajectory from the same part of the slit at the ν th generation. Using the above recursion relation, the exact specular collision numbers for 3^ν trajectories at any generation ν can then be obtained for $\phi = 45^\circ$.

III. RESULTS AND DISCUSSIONS

The collision numbers and their spatial distribution along the slit are computed for the 7th and 8th pre-fractal generation ($\nu = 7$ and 8). A number of $N_{tot} = 3^\nu$ equally spaced particles are launched from the slit. The spatial distribution of the collision numbers is studied under two different conditions. Firstly, the distribution of the specular collision numbers at 45° angle of incidence for which the exact collision numbers are available, is investigated. Secondly, the effect of the surface micro-roughness (Γ) on the collision spectrum is studied for the same slit angle. In this case, the collision spectrums are averaged over 160 samples. The general quality of the numerical results is verified with the exact collision spectrum for $\phi = 45^\circ$ and $\Gamma = 0^\circ$ obtained from the recursion relation (Eq. 3).

Before discussing the multifractality associated with the spatial distribution of the collision numbers, it is important to consider their statistical distributions. The probability to have a trajectory with N collisions is measured by

$$P_N = \frac{n_N}{N_{tot}} \quad (4)$$

where n_N is the number of trajectories having N collisions and N_{tot} is the total number of trajectories. The distribution of P_N for different Γ in Fig. 3. It can be observed that most of the trajectories exhibit between 3 and 9 collisions. A large number of trajectories then leave the pre-fractal surface making only a few collisions and only a few trajectories make a large number of collisions. It is important to note that the roughness Γ has little effect on the collision number distribution except the reduction in the maximum number of collisions with increasing Γ . The total number of collisions is also very weakly dependent on the randomness Γ . These features have already been observed in the case of interaction of ballistic trajectories with pre-fractal pores [10] in the Knudsen diffusion regime where the collision number distribution was found to be of the Lévy type. However, up to the 8th pre-fractal generation, no simple power law distribution of the collision numbers was found.

To study the multifractal aspect of the trajectory distribution, a collision spectrum is obtained. The collision spectrum is a distribution of the relative collision numbers of the trajectories over the slit. The relative collision number $\mu(x)$ of a particle trajectory originating from a position x on the slit and making $n(x)$ collisions with the surface is given by

$$\mu(x) = \frac{n(x)}{\sum_x n(x)} \quad (5)$$

where the sum is over all the particles. This normalized collision number is the measure under study here. In Fig. 4, $\mu(x)$ is plotted against the initial particle position keeping $\Gamma = 0$ (specular reflection) for $\nu = 7$. The value of $\mu(x)$ is represented by impulses at the initial positions x . The spectrum is symmetrical around the central position, as expected. Most interesting to note, this spectrum corresponds to a uniform exploration of the irregular surface as there is a single collision per segment (see Fig. 2). The maximum number of collisions made by the central trajectory is 3^7 and the total number of collisions made by all the particles is 5^7 (the first generation has 5 collisions) at $\nu = 7$. Thus, μ_{max} is given by $\mu_{max} = 3^7/5^7 \approx 0.03$, as found numerically.

The collision spectrums obtained in the presence of surface micro-roughness, $\Gamma = 2^\circ$ (a), $\Gamma = 6^\circ$ (b), and $\Gamma = 10^\circ$ (c) are shown in Fig. 5 for the $\nu = 7$ th pre-fractal generation. Due to micro-roughness, the spectrums become more uniform and the value of μ_{max} is decreased with respect to the specular value. The value of μ_{max} is decreasing with increasing Γ as it is also seen in the collision number distribution (Fig. 3) that the maximum number of collisions is decreasing with Γ .

To show the multifractal nature of the distribution $\mu(x)$, it is necessary to study the scaling of the q -moments of the measure over different length scales on the slit. If the measure $\mu(x)$ is multifractal and the slit is divided into n_ϵ boxes of size ϵ , then the weighted number of boxes $N(q, \epsilon)$ is given by

$$N(q, \epsilon) = \sum_{i=1}^{n_\epsilon} \mu_i^q \approx \epsilon^{-\tau(q)} \quad (6)$$

where μ_i is the sum of the relative collision number of trajectories initiated in the i th box. Here $\tau(q)$ is called the ‘‘collision exponent’’. In Fig. 6, the values of $\tau(q)$, obtained by the box counting method, are plotted against q for $\nu = 7$ (circle) and 8 (square) with $\Gamma = 0$ (specular reflections). The values of $\tau(q)$ do not depend on ν , the macro-irregularity of the surface. Note that, $\tau(0)$ is ≈ 1 and $\tau(1)$ is ≈ 0 here. $\tau(0)$ corresponds to the dimension of the slit which is 1 here and $\tau(1)$ is zero because $\sum_x \mu(x) = 1$. The fact that a sequence of exponents are obtained irrespective of the generation ν confirms the multifractal nature of the spectrum. Note that the multifractality obtained for the specular collision spectrum at 45° angle of incidence corresponds to a uniform exploration of the irregular surface (Fig. 2). Consequently, a measure defined over the irregular surface instead of the slit will not exhibit multifractality.

A check of the validity of our numerical computations can be made for the case $\phi = 45^\circ$ with specular reflections. In that case there exists a trinomial multiplicative cascade [15]. A comparison between the collision spectrum and the multiplicative cascade is made here. At the zeroth generation of the cascade $k = 0$, a uniform distribution of unit mass over an interval $[0,1]$ is considered. In the next generation $k = 1$, the unit mass is distributed over three equal intervals $[0, 1/3]$, $[1/3, 2/3]$, and $[2/3, 1]$ with weighted probabilities $p_0 = 1/5$, $p_1 = 3/5$, and $p_2 = 1/5$ similar to the collision number distribution over the slit at $\phi = 45^\circ$. At $k = 7$ generation, the mass distribution will be exactly the same as the collision number distribution over the slit obtained for $\nu = 7$ generation of the pre-fractal surface. The measure over the unit interval remains always conserved in the iteration process since $\sum p_i = 1$. The mass exponent $\tau_m(q)$ can be calculated in terms of p_i as

$$\tau_m(q) = \lim_{k \rightarrow \infty} \frac{\ln[p_0^q + p_1^q + p_2^q]^k}{\ln 3^{-k}} = -\frac{\ln[p_0^q + p_1^q + p_2^q]}{\ln 3}. \quad (7)$$

The solid line in Fig. 6 represents the mass exponent $\tau_m(q)$ for this trinomial mass distribution. With no surprise, there exists an excellent agreement between the exponents for the specular collision number distribution at $\phi = 45^\circ$ and the trinomial mass distribution.

The effect of micro-roughness (Γ) on the collision exponents is discussed now. In Fig. 7, $\tau(q)$ is plotted against q for $\Gamma = 2^\circ$ (circle), 6° (square), and 10° (triangle). The solid line represents the collision exponents for $\Gamma = 0^\circ$, the specular reflections. At large positive q , the micro-roughness Γ has a significant effect on $\tau(q)$ with respect to $\Gamma = 0^\circ$. It is expected because the spectra change with Γ . Again a sequence of collision exponents $\tau(q)$ is obtained whatever the micro-roughness Γ . This means that the spectrum are still of multifractal nature.

To determine the nature of the multifractality, the dimensions $f(\alpha)$ are obtained as usual as a function of the Lipschitz-Hölder exponent α through a Legendre transformation [15]

$$\alpha(q) = -\frac{d}{dq}\tau(q), \quad f(\alpha) = q\alpha(q) + \tau(q) \quad (8)$$

of the sequence $\tau(q)$. The curve $f(\alpha)$ for specular reflexions is discussed first. In Fig. 8, it is represented by circles. The solid line represents $f(\alpha)$ for the trinomial mass distribution. Naturally, there is a good agreement between $f(\alpha)$ of specular collision distribution and the trinomial mass distribution. Since the slit here is a one dimensional object, the $f(\alpha)$ curves are always ≤ 1 and $f_{max}(\alpha)$ is equal to 1. One observes two parabolas in the $f(\alpha)$ curve. This means that the multifractal is of trinomial nature. The values of α_{min} and α_{max} for specular reflections at $\phi = 45^\circ$ can be predicted. The increment in the measure over a length ξ to $\xi + \delta$ is $\mu_\xi = \mu(\xi + \delta) - \mu(\xi)$. The Lipschitz-Hölder exponent $\alpha(\xi)$ is defined as $\mu_\xi = \delta^{\alpha(\xi)}$. After n th iteration, $\delta = 1/3^n$ and $\alpha(\xi)$ is given by

$$\alpha(\xi) = \frac{\ln \mu_\xi}{\ln \delta} = -\frac{\frac{\xi}{2} \ln p_0 + (1 - \xi) \ln(1 - p_0 - p_2) + \frac{\xi}{2} \ln p_2}{\ln 3} \quad (9)$$

where $p_0 = p_2 = 1/5$ and $p_1 = 1 - p_0 - p_2 = 3/5$ for the case considered here. α_{min} and α_{max} correspond to $\xi = 0$ and $\xi = 1$ respectively and they are obtained as $\alpha_{min} = -\ln(3/5)/\ln 3 \approx 0.465$ and $\alpha_{max} = -\ln(1/5)/\ln 3 \approx 1.465$. These two extreme values are marked by two crosses on the α -axis. It can be seen that α_{min} and α_{max} obtained numerically for the specular collision spectrum at $\phi = 45^\circ$ are very close to the predicted values. Note that, as expected, the whole $f(\alpha)$ versus α is independent of the generation ν of the pre-fractal surface. This is shown in Fig. 8, where the data for $\nu = 7$ (circles) and $\nu = 8$ (squares) collapse onto the same curve. It is also interesting to notice that α_{max} is exactly equal to the dimension $\ln 5/\ln 3$ of the pre-fractal and $\alpha_{min} = \alpha_{max} - 1$. These features are specific of the prefractal geometry and the angle of incidence considered here.

Always in the case of specular reflections, but for other angles of incidence like $\phi = 30^\circ$ and 60° , it is found that the $f(\alpha)$ versus α curves also consist of two parabolas. However, in both cases, the values of α_{min} and α_{max} keep on changing with the generation ν upto 8th generation. This is attributed to the fact that the multiplicative process in these cases is more involved than in the case of 45° incidence. There should exist for these cases a cascade of different sequential values of p_0 , p_1 and p_2 so that the asymptotic multifractal measure is still not reached for $\nu = 8$.

The effect of micro-roughness of the surface on the $f(\alpha)$ curve is discussed now. In Fig. 9, $f(\alpha)$ versus α curves are plotted for $\Gamma = 2^\circ$ (circles), 6° (squares), and 10° (diamonds) at $\phi = 45^\circ$ and $\nu = 7$. The solid line represents the $f(\alpha)$ curve for specular collisions. The triangles represent the results for an hypothetic ‘‘totally’’ diffusing surface for which re-emission would be isotropic, *i.e.*; occurring randomly in any direction between -90° to 90° with respect to the normal, independent of the angle of incidence. This is equivalent to the $\Gamma \rightarrow 90^\circ$ limit. There are two important things to note. First, the micro-roughness (or random character of the particle re-emission) of the surface is unable to destroy either the multifractality or the trinomial nature of the multifractality even at the maximum possible value of Γ , corresponding to the ‘‘totally diffusing surface’’. Second, the values of α_{min} depends strongly on the

degree of surface roughness Γ whereas α_{max} remains almost constant. The value of α_{min} increases as a function of Γ . This is expected. As Γ increases, the value of μ_{max} decreases, the spectrum becoming more uniform as seen in Fig. 5 and the smaller value of μ_{max} corresponds to the larger value of α_{min} . The value of α_{max} could also be estimated from the knowledge of the minimum measure μ_{min} . For a single realization, the total number of collisions is $\approx 10^5$. Thus, $\mu_{min} \approx 1/10^5$ (for a trajectory having a single collision) and the value of α_{max} is then given by $\ln \mu_{min} / \ln \delta = \ln(1/10^5) / \ln(1/3^7) \approx 1.497$ very close to what is obtained here. Since the value of μ_{min} is almost independent of the surface roughness (total number of collisions almost independent of Γ) in this collision process, the value of α_{max} remains unchanged.

From these results, it is found that the multifractality as well as the trinomial nature of the multifractality associated with this collision process remains unaltered irrespective of the surface micro-roughness. This is because, the multifractality of the collision spectrum is the outcome of a multiplicative cascade of the spatial sub-distributions which are independent of the various situations considered here. The trinomial nature of the multifractal is due to the type of pre-fractal chosen here to model the surface macro-irregularity: a quadratic Koch curve, each element being divided into three elements in the next generation. A different pre-fractal generator, *i.e.*; a different model of surface macro-irregularity will then lead to a different multifractal behavior.

The information dimension [16] is the value of $f(\alpha)$ when $f(\alpha) = \alpha$. The information dimension D_I is found to be $D_I \approx 0.854$ for 45° angle of incidence with $\Gamma = 0$ and at $\nu = 7$. This indicates that the measure is supported by a minor fraction of the particle trajectories. This also illustrates the fact that most of the trajectories interacts weakly with the fractal surface. Interestingly, the information dimension increases with the random character of the particle-surface interaction. Indeed for $\Gamma = 2^\circ, 6^\circ$ and 10° the values of information dimensions are $D_I \approx 0.877, 0.934$ and 0.952 respectively. For the diffused surface $D_I \approx 0.964$. This corresponds to more and more uniform collision number distribution on the slit.

It is interesting to comment on the uniform exploration of the surface, each element receiving the same number of particles at least for an angle of incidence of 45 degrees. This is analogous to the results obtained by Andrade et al [17] through a molecular dynamics study of Knudsen diffusion in the same geometry. In this last case, it is the first collision that is uniformly distributed over the perfectly absorbing surface whereas here, the surface is perfectly reflecting. The uniform exploration found in these both cases constitutes a qualitative evidence of the absence of screening in Knudsen diffusion. It can be considered as a remarkable fact that, seen from the source of particles, the collision numbers are strongly non-uniform, while seen from the surface the exploration is uniform. This may have interesting consequences for catalyst deactivation which should also be uniformly distributed.

IV. CONCLUSION

The collision number distribution and their spatial behaviour are obtained for $2D$ ballistic particles interacting with a pre-fractal curve of dimension $\ln 5 / \ln 3$. The trajectories considered here correspond to the Knudsen diffusion regime. The micro-roughness of the surface, or the random character of the particle-surface interaction, is included through a randomness parameter Γ in the reflection angle. It is found that most of the particles make only a few collisions whereas a few trajectories exhibit a large number of collisions. A multifractal measure of the spectrum is defined in terms of the relative collision number over a linear slit from which the trajectories are launched. A sequence of ‘‘collision exponents’’ $\tau(q)$, is determined by the box counting method and it is found that the sequence depends on the moment q . Thus, the spatial distribution of the collision numbers is a multifractal spectrum. The fractal dimensions $f(\alpha)$ depend on the random character of the particle re-emission (Γ). Irrespective of the values of Γ , the plot of $f(\alpha)$ versus Lipschitz-Hölder exponent α consist of two parabolas. The spectrum is then that of a multiplicative trinomial multifractal independent of surface micro-roughness. The information dimension D_I of the measure is found to be smaller than 1 and increases with the random character of the particle surface interaction. Different type of surface macro-irregularity would lead to different multifractal behavior. Notably, the surface however works uniformly, indicating an absence of screening in the Knudsen diffusion regime.

-
- [1] B. B. Mandelbrot in *Statistical Model of Turbulence* edited by M. Rosenblatt and C. Van Atta, Lecture notes in Physics, **12**, (Springer, New York, 1972).
 - [2] F. Milde, R. A. Römer, and M. Schreiber, Phys. Rev. B **55**, 9463 (1997); B. Huckestein and R. Klesse, Phil. Mag. B **77**, 1181 (1998); S. M. Nishigaki, Phys. Rev. E. **59**, 2853 (1999).
 - [3] J. P. Bouchaud, M. Potters, M. Meyer, Eur. Phys. J. B **13**, 595 (2000); J-F Muzy, D. Sornette, J. Delour, and A. Arneodo, Quantitative Finance, **1**, 131 (2001).

- [4] P. Ch. Ivanov, L. A. Nunes Amaral, A. L. Goldberger, S. Havlin, M. G. Rosenblum, Z. Struzik, H. E. Stanley, *Nature*, **399**, 451 (1999).
- [5] K. Kim, J. S. Choi, and Y. S. Kong, *J. Phys. Soc. Jpn.* **67**, 1583 (1998); K. Kim, G. H. Kim, and Y. S. Kong, *Fractals*, **8** 181 (2000).
- [6] B. B. Mandelbrot, *The Fractal Geometry of Nature* (W. H. Freeman, New York, 1982); B. Sapoval, *Fractals* (Aditech, Paris, 1989) and *Universalités et Fractales* (Flammarion, Paris, 1997).
- [7] M. Knudsen, *Ann. Phys. (N.Y.)* **28**, 75 (1909).
- [8] J. M. Thomas and W. J. Thomas, *Principle and Practice of Heterogeneous Catalysis* (VCH, Weinheim, 1997); G. F. Froment and K. B. Bischoff, *Chemical Reactor Analysis and Design* (John Wiley and Sons, New York, 1990).
- [9] V. Pasquier, P. Lévitiz, and A. Delville, *J. Phys. Chem.* **100**, 10249 (1996).
- [10] S. B. Santra and B. Sapoval, *Phys. Rev. E* **57**, 6888 (1998); S. B. Santra, B. Sapoval, and O. Haeblerlé, in *Frctals in Engineering: From Theory to Industrial Applications*, edited by J. Lévy-Vehel, E. Lutton, and C. Tricot (Springer, London, 1997).
- [11] K. Malek and M.-O. Coppens, *Phys. Rev. Lett.* **87**, 125505 (2001) and references therein.
- [12] S. Feng and L. Golubovic, *Phys. Rev. Lett.* **65**, 1028 (1990); L. Golubovic, S. Feng, and F. Zeng, *Phys. Rev. Lett.* **67**, 2115 (1991); J. P. Bouchaud, D. Touati, and D. Sornette, *Phys. Rev. Lett.* **68**, 1787 (1992).
- [13] J. Feder, *Fractals* (Plenum Press, New York and London, 1988).
- [14] J. P. Valteau, D. J. Diestler, M. Schoen, A. W. Hertzner, and M. E. Riley, *J. Chem. Phys.* **95**, 6194 (1991).
- [15] C. J. G. Evertsz and B. B. Mandelbrot in the appendix of *Chaos and Fractals* by H. O. Peitgen, H. Jürgens, and D. Saupe (Springer, New York, 1992).
- [16] P. Grassberger, *Phys. Lett. A* **97**, 227 (1983); H. G. E. Hentschel and I. Procaccia, *Physica D* **8**, 435 (1983).
- [17] J. S. Andrade Jr, H. F. Silva, M. Baquil, and B. Sapoval, *Phys. Rev. E* **68**, 041608 (2003).

Number of Collisions															
$\nu = 0$	1														
$\nu = 1$	1			3			1								
$\nu = 2$	1	3	1	3	9	3	1	3	1						
$\nu = 3$	1	3	1	3	9	27	9	3	1	3	9	3	1	3	1

TABLE I: Number of specular collisions made by ballistic trajectories incident at 45° and interacting with a quadratic Koch curve of dimension $\ln 5/\ln 3$ at different generations ν . The number of collisions at a generation $\nu + 1$ is given by $n_\nu \times (1, 3, 1)$ where n_ν is the number of collisions in the previous generation for the same trajectory.

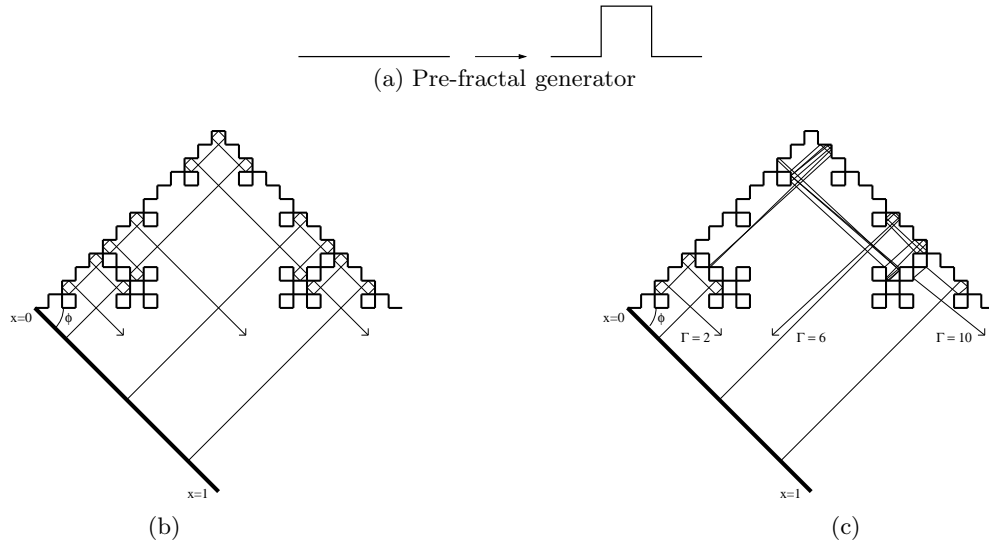


FIG. 1: Schematic representation of the collision process at the third generation of the pre-fractal surface, a quadratic Koch curve of dimension $\ln 5/\ln 3$. The generator of the pre-fractal is shown in (a). The thick lines, extended from $x = 0$ to $x = 1$, in (b) and (c) represent the slit. The slit angle ϕ is 45° here. In (b), the trajectories of particles with specular reflections from three different positions on the slit are shown. The central trajectory makes $3^3 = 27$ collisions and the other two make 9 collisions each. The trajectories of non specular reflection are shown in (c). These trajectories are generated for $\Gamma = 2, 6$ and 10 for the same initial positions x and slit angle ϕ of (b).

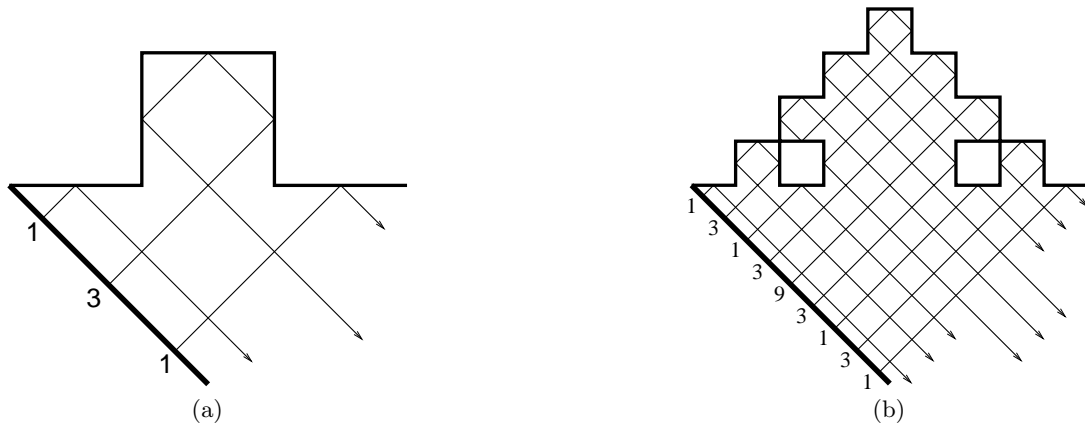


FIG. 2: Multiplication of specular collision numbers from $\nu = 1$ generation of the pre-fractal (a) to $\nu = 2$ generation of the pre-fractal (b) at $\phi = 45^\circ$. Note that the collision numbers are uniformly distributed over the pre-fractal surface, each segment has one collision.

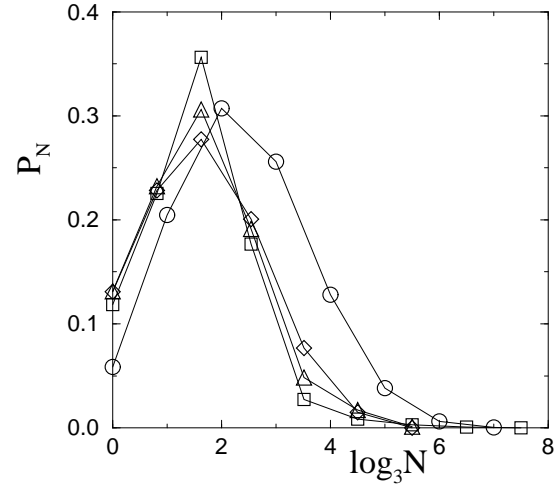


FIG. 3: Collision number distribution P_N versus N . The distributions are given for $\Gamma = 0$ (circles) specular reflection, 2° (squares), 6° (triangles), and 10° (diamonds) at 45° slit angle. The distribution shows that most of the particles make few collisions while a few trajectories exhibit a very large number of collisions. Note the existence of a tail in the distribution.

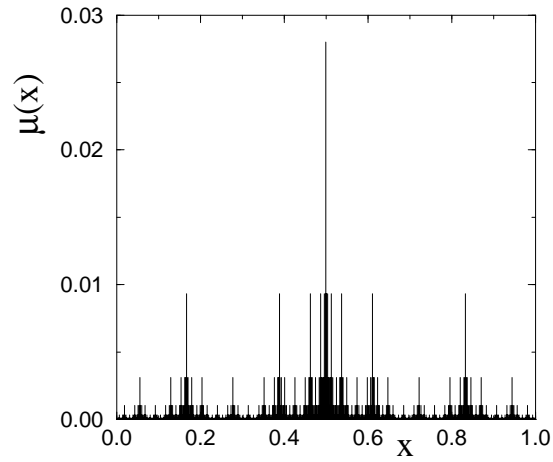


FIG. 4: Plot of the relative collision numbers $\mu(x)$ versus x , initial position on the slit, for $\Gamma = 0^\circ$ specular reflections. This “specular” spectrum is symmetric around the central position as it is expected.

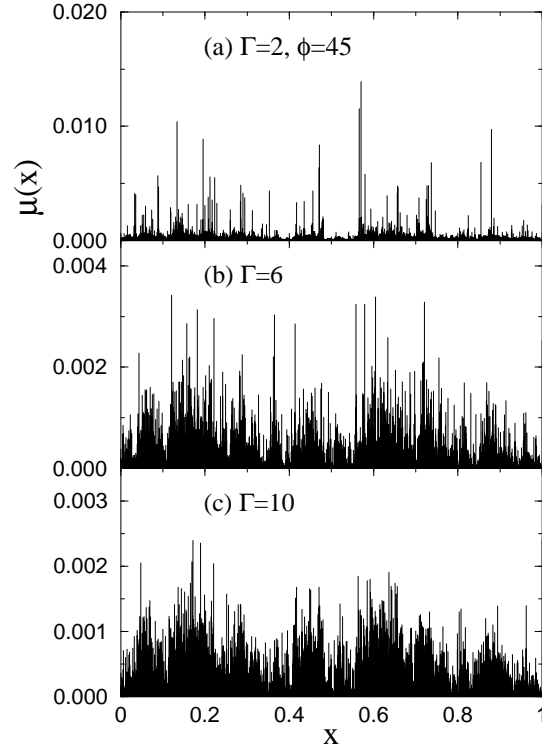


FIG. 5: Plot of relative collision numbers $\mu(x)$ as a function of the initial position (x) on the slit for (a) $\Gamma = 2^\circ$, (b) $\Gamma = 6^\circ$, and (c) $\Gamma = 10^\circ$. Note the general decrease of the values and the increased spreading of the distribution as Γ increases.

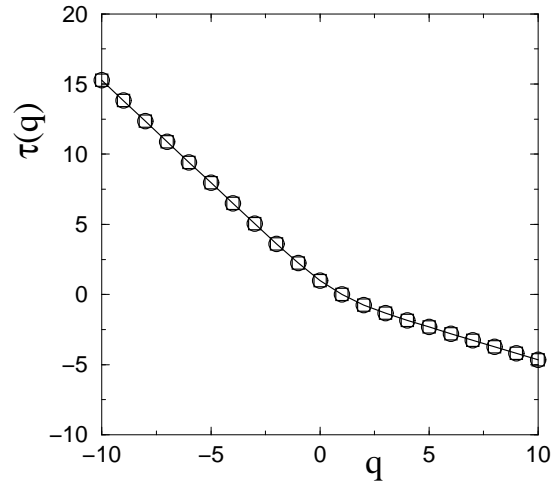


FIG. 6: Plot of the numerical $\tau(q)$ against q for different generations $\nu = 7$ (circles) and $\nu = 8$ (squares) with $\Gamma = 0$. The collision exponents remains almost the same. The solid line represents the theoretical $\tau_m(q)$ for the trinomial mass distribution.

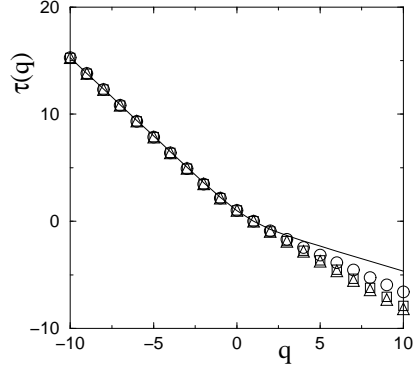


FIG. 7: Plot of $\tau(q)$ against q for $\Gamma = 2$ (circles), $\Gamma = 6$ (squares), and $\Gamma = 10$ (triangles) at 45° slit angle. The solid line represents $\tau(q)$ for the specular collisions. The randomness factor Γ has a significant effect on $\tau(q)$ for large positive q values.

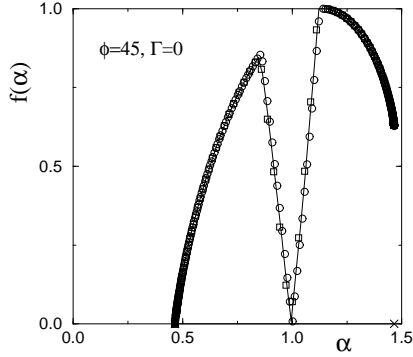


FIG. 8: Plot of $f(\alpha)$ against the Lipschitz-Hölder exponent α for specular collisions at $\nu = 7$ (circles) and $\nu = 8$ (squares). The crosses represent the values of α_{min} and α_{max} and the solid line represents $f(\alpha)$ for trinomial mass distribution. The curves are identical.

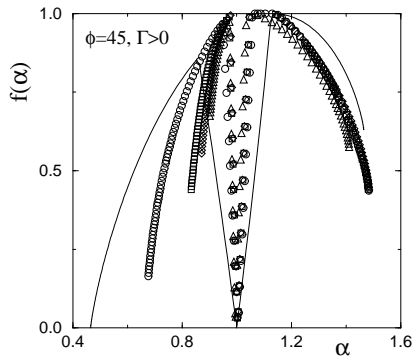


FIG. 9: Plot of $f(\alpha)$ against α for different Γ at $\phi = 45^\circ$: circles for $\Gamma = 2^\circ$, squares for $\Gamma = 6^\circ$ and diamonds for $\Gamma = 10^\circ$. Triangles correspond to the totally diffusing surface and the solid line corresponds to $f(\alpha)$ of the trinomial mass distribution.